Yb-doped Y-Al-O thin films with a self-organized columnar structure and their anti-Stokes photoluminescence properties

Nakayama, Y. ; Nakagawa, N. ; Matsuo, Y. ; Kaizu, T. ; Harada, Y. ; Ishihara, T. ; Kita, T.

(Citation)
AIP Advances,12(2):025110

(Issue Date)
2022-02-01

(Resource Type)
journal article

(Version)
Version of Record

Yb-doped Y–Al–O thin films with a self-organized columnar structure and their anti-Stokes photoluminescence properties

Cite as: AIP Advances **12**, 025110 (2022); https://doi.org/10.1063/5.0079632
Submitted: 01 December 2021 • Accepted: 20 January 2022 • Published Online: 04 February 2022

Y. Nakayama, N. Nakagawa, Y. Matsuo, et al.

Yb-doped Y–Al–O thin films with a self-organized columnar structure and their anti-Stokes photoluminescence properties

Cite as: AIP Advances 12, 025110 (2022); doi: 10.1063/5.0079632
Submitted: 1 December 2021 • Accepted: 20 January 2022 •
Published Online: 4 February 2022

Y. Nakayama,[1,a] N. Nakagawa,[2] Y. Matsuo,[1] T. Kaizu,[1] Y. Harada,[1,a] T. Ishihara,[3] and T. Kita[1]

AFFILIATIONS

[1] Department of Electrical and Electronic Engineering, Graate School of Engineering, Kobe University, 1-1 Rokkodai, Nada, Kobe 657-8501, Japan
[2] Department of Electrical and Electronic Engineering, Faculty of Engineering, Kobe University, 1-1 Rokkodai, Nada, Kobe 657-8501, Japan
[3] Hyogo Prefectural Institute of Technology, 3-1-12 Yukihira, Suma, Kobe 654-0037, Japan

[a] **Authors to whom correspondence should be addressed:** 179t250t@stu.kobe-u.ac.jp and y.harada@eedept.kobe-u.ac.jp

ABSTRACT

We fabricated ytterbium-doped yttrium aluminum oxide (Yb:Y–Al–O) thin films by radio-frequency magnetron sputtering and evaluated their crystallinity and anti-Stokes photoluminescence (PL) properties for optical refrigeration. The Yb:Y–Al–O films that were grown on c-sapphire substrates had better transparency than the films deposited on fused-quartz substrates. The better transparency is considered to be a result of the smaller mismatch between the thermal expansion coefficients of Yb:Y–Al–O and c-sapphire. We found that the thin films on the c-sapphire substrates consist of densely packed sub-micron columnar crystals that are aligned perpendicular to the substrate. In these films, we confirmed the existence of perovskite, garnet, and monoclinic phases despite using a single-phase sputtering target. The excitation wavelength dependence of anti-Stokes PL is used to investigate the energy transfer process between trivalent Yb ions in neighboring columnar crystals. The data indicate that the resonant energy transfer from Yb^{3+} ions at a specific seven-coordinated site of the monoclinic phase to Yb^{3+} ions in neighboring columnar crystals is faster than the radiative relaxation at the energy-donor site.

I. INTRODUCTION

Laser cooling in solids can be realized if phonon-assisted anti-Stokes photoluminescence (PL) is efficiently extracted from a luminescent material and heat generation processes are sufficiently suppressed in this material.[1] Such optical cryocoolers are able to refrigerate an object without heat generation near the cooling target.[2] In 2018, an all-solid-state optical cryocooler that can cool an HgCdTe sensor of a Fourier transform infrared spectrometer to 135 K was demonstrated for the first time.[3] The advantages of optical cryocoolers, such as no vibration, no electromagnetic perturbations near the cooling target, and a smaller cryostat, are considered to be even useful for small low-earth-orbiting satellites.[4] Radiation balanced lasers (RBLs) are another interesting application area where the laser cooling process is used to overcome the thermal degradation problem:[5] In conventional laser light sources, thermal degradation is unavoidable (due to the operating principle), but at the radiation-balanced point of an RBL, the heat generated by Stokes and other non-radiative processes is carried away by anti-Stokes PL. If the heat reduction by anti-Stokes PL is stronger than the heat generation, net-cooling occurs, and a self-cooling laser can be realized.

So far, in the field of laser cooling of solids, III–V semiconductors, lead halide perovskites, and rare earth (RE)-doped materials have been mainly investigated.[6–9] RE-doped materials are known to be good candidates for laser cooling in particular,[10] and some of them have been shown to cool down to less than 285 K under moderate excitation conditions, such as 1.8 W at 1030 nm.[1,6,11–13] In

terms of suppressing multi-phonon relaxation processes in excited RE-doped materials, a low maximum phonon energy and a large first-excited-state energy (or energy gap) are considered important.[14] Among RE elements, the trivalent ytterbium (Yb) ion has the second largest energy gap of ~10 000 cm^{-1}. Therefore, Yb^{3+} ions have been doped into various oxides and fluoride host materials with a low maximum phonon energy.[15]

One of the representative materials for laser cooling is Yb-doped yttrium lithium fluoride. Because of its low maximum phonon energy of 420 cm^{-1}, this material was used in the first demonstration of an all-solid-state optical cryocooler,[3] and net-cooling from room temperature to cryogenic temperatures below 100 K has been demonstrated.[16] An Yb-doped yttrium aluminum garnet (Yb:YAG) crystal was used as the gain medium in the first demonstration of continuous-wave (CW) RBL operation.[17] Recently, we have proposed that a higher RBL gain than Yb:YAG can be realized in Yb-doped yttrium aluminum perovskite (Yb:YAP), which belongs to the family of yttrium aluminum oxide crystals with a low maximum phonon energy (620 cm^{-1})[18] and strong light absorption.[19] However, the net-cooling of Yb:YAP has not yet been observed due to the strong scattering loss at the rough surface and contaminants in the ceramic sample.

Net-cooling requires material purification and several optimizations, such as maximizing the extraction efficiency of anti-Stokes PL.[20,21] In the same way as the demonstration of laser cooling in RE-doped nano-crystals[22] and fibers,[23] the demonstration of laser cooling in thin films should be possible in the future if appropriate material processing technologies can be developed. In this work, we fabricated transparent thin films of Yb-doped yttrium aluminum oxide (Yb:Y–Al–O) by radio-frequency magnetron sputtering and evaluated their crystallinity and anti-Stokes PL properties. Three crystal phases (garnet, monoclinic, and perovskite phases) were observed despite the use of a single-phase (perovskite) yttrium aluminum polycrystal sputtering target. The transparent Yb:Y–Al–O thin films grown on c-sapphire substrates have a dense and uniform columnar structure formed by a self-organization process and contain nano-pillars of garnet and monoclinic crystals. Reflecting this unique structure, the Yb:Y–Al–O thin films show unique PL characteristics that differ from those of single-phase crystals.

II. MATERIALS AND METHODS

Yb:Y–Al–O thin films were deposited on c-sapphire and fused-quartz substrates by radio-frequency magnetron sputtering with mixed Ar/O_2 gas (Ar/O_2 = 1) and Yb:YAP ceramic targets (Yb_2O_3/Y_2O_3 molar ratio = 0.06 and diameter = 50 mm) fixed on a cathode (PGS-152K, Kenix Co., Ltd.). The background pressure in the sputtering chamber was 6.6×10^{-4} Pa, and the pressure during sputtering was 1.0 Pa. The temperature of the substrate during film deposition was ~200 °C. The as-deposited films were annealed for crystallization in an air atmosphere at 1000 °C for 10 h in an electric furnace. The film thickness was measured by a three-dimensional optical profilometer that uses white-light interferometry (Profilm3D, Filmetrics Inc.).

The different crystal phases in the annealed films were determined by analyzing the x-ray diffraction (XRD) patterns (UltimaIVProtectus, Rigaku Corp.). The integrated x-ray powder diffraction software PDXL (Rigaku Corp.) and the data from the International Center for Diffraction Data (ICDD) were used to perform the Rietveld refinement. The surface morphologies of the films were evaluated by using an optical microscope and scanning electron microscopy (SEM) measurements (JSM-7100F, JEOL Ltd.).

To obtain the PL spectra under indirect excitation conditions of the Yb^{3+} ions, a laser diode operating at 405 nm (3.06 eV) was used. This indirect excitation is useful to confirm the basic PL characteristics of the material. A tunable CW laser [full width at half-maximum (FWHM): 1.2 nm] was employed in the anti-Stokes PL and PL excitation (PLE) image measurements. For the site-selective PLE image measurement, light from a supercontinuum source was passed through a double monochromator. The obtained monochromatic light had an FWHM of 1.5 nm. The fluorescence of the sample was dispersed by a single monochromator (F-number: 3.88, grating with 600 lines/mm, and a blaze wavelength of 1000 nm) and detected by an InGaAs diode array. The spectral intensity of the PLE image was normalized by the excitation photon number.

III. RESULTS AND DISCUSSION I: BASIC PROPERTIES

A. Phase separation in Yb:Y–Al–O thin films

Figure 1(a) shows the XRD patterns of 1.0-μm-thick annealed Yb:Y–Al–O thin films on c-sapphire (upper panel) and fused-quartz (middle panel). The dotted, solid, and dashed arrows labeled "M," "G," and "P" indicate the XRD peaks of the monoclinic, garnet, and perovskite phases, respectively. For this assignment, we used the data from the ICDD shown at the bottom of Fig. 1(a), which present the standard relative diffraction intensities of yttrium aluminum monoclinic (YAM) and YAG. The strong XRD peak signals for the Yb:Y–Al–O film on c-sapphire at 38° and 42° are due to the substrate. The influence of annealing on the crystallinity of the Yb:Y–Al–O thin film has been confirmed by XRD measurement. The XRD patterns of annealed (red) and as-sputtered (black) Yb:Y–Al–O thin films (thickness: 0.2 μm) on the fused-quartz substrate shown in Fig. 1(b) indicate that the Yb:Y–Al–O crystal could not be obtained without annealing. This long-range ordering in the thin film as a result of the annealing is thickness independent. Similarly, the PL of the Yb:Y–Al–O film could not be observed in the as-sputtered sample.

In the range of 16–40 degrees shown in Fig. 1(a) for the annealed Yb:Y–Al–O film on the fused-quartz substrate, we can confirm a halo pattern that originates from an amorphous structure of the substrate. All the observed XRD peak signals are confirmed to be attributed with garnet, monoclinic, and perovskite phases. Both annealed films show strong XRD peaks of garnet and monoclinic phases. Hence, we confirmed a phase separation in the prepared thin films, and they consist mainly of garnet and monoclinic crystals. From the Rietveld refinement of the data of Yb:Y–Al–O/c-sapphire samples with different film thicknesses (Table I), we found that the degree of phase separation is stronger for thinner films. On the other hand, the 6.9-μm-thick film had a dominant contribution of YAG (74 wt. % YAG, 12 wt. % YAM, and 14 wt. % YAP). Thus, at the beginning of the crystallization of the sputtered Yb:Y–Al–O film during the annealing process, there are garnet, monoclinic, and perovskite crystal cores, and the rate of crystallization of the garnet phase is higher than that of the monoclinic phase.

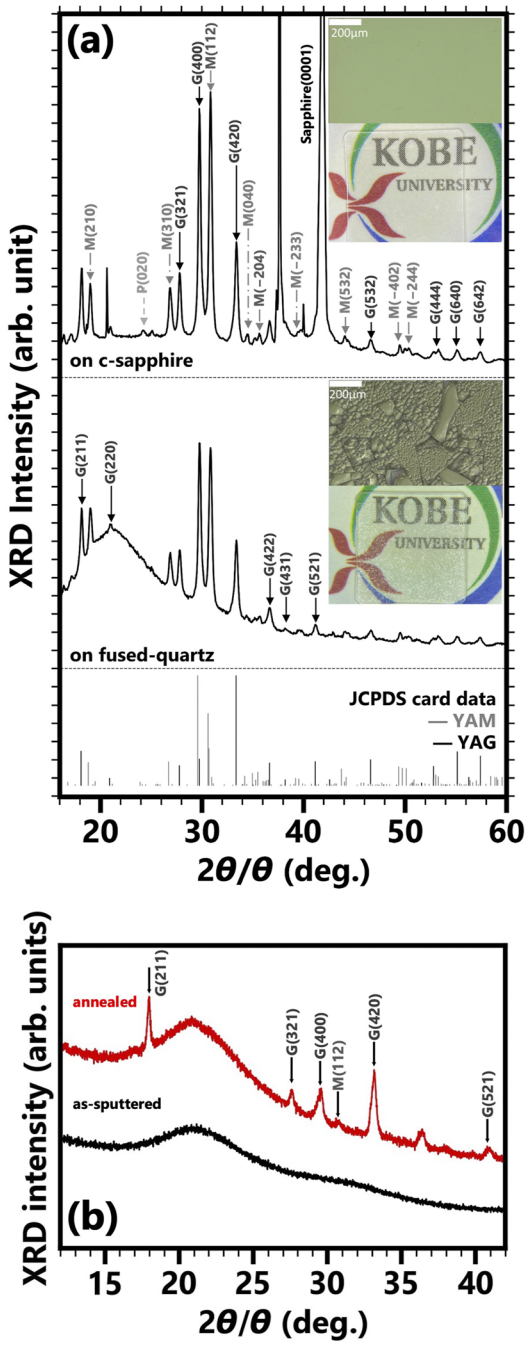

FIG. 1. (a) XRD patterns of 1.0-μm thick annealed thin films prepared on c-sapphire (top panel) and fused-quartz substrates (middle panel). The dotted, solid, and dashed arrows labeled "M," "G," and "P" indicate the XRD peaks of the monoclinic, garnet, and perovskite phases, respectively. The dotted and solid lines at the bottom panel indicate the relative diffraction intensities of polycrystalline YAM and YAG powders recorded in the ICDD. The insets show the optical microscope images and the macroscopic appearances of the samples. The dotted lines are baselines corresponding to zero intensity. (b) XRD patterns of annealed (red) and as-sputtered (black) Yb:Y–Al–O thin films grown on fused-quartz substrate. The film thickness is 0.2 μm.

TABLE I. The film-thickness dependence of the weight ratios of YAG, YAM, and YAP estimated by Rietveld refinement for annealed Yb:Y–Al–O on c-sapphire. G, M, and P indicate the garnet, monoclinic, and perovskite phases, respectively.

Yb:Y–Al–O film thickness (μm)	Ratio G:M:P (wt. %)
0.2	42:51:7
1.4	47:42:11
3.0	67:22:10
5.0	61:24:15
6.9	74:12:14

For an RBL application, the perovskite phase is preferred due to its superior properties as an RBL gain medium. From the well-known atomic mass dependence of the sputtering rate, gently decreasing the Al/Y ratio of the sputtering target to less than 1.0 is promising to obtain Yb:$YAlO_3$. This approach is known to be effective for Ce-doped YAG, an LED phosphor material.[24]

B. Improved transparency

The insets in Fig. 1(a) show the optical microscope images and the macroscopic appearance of the annealed samples. The thin film on the c-sapphire substrate has no cracks and a high transparency, whereas many cracks were observed in the thin film grown on the fused-quartz substrate. The thermal expansion coefficients of Yb:YAG, sapphire, and fused-quartz are ~10^{-6},[25] ~10^{-6},[26] and ~10^{-7} K^{-1},[27] respectively. Therefore, the large difference between the thermal expansion coefficients of Yb:Y–Al–O and the fused-quartz substrate induces a high in-plain strain in the film during the cooling process (after annealing), and strain relaxation occurs by crack formation.

In laser cooling of solids, a low density of unexpected heat sources such as OH^- is essential.[6] In addition, weak scattering at the surface of the cooling material is also preferable. Because cracks induce scattering of excitation light and can generate unexpected heat sources by dangling bonds, Yb:Y–Al–O on c-sapphire is considered to be a more suitable material–substrate combination.

C. Morphology

The morphology of a film reflects the growth process and thus provides us with more information about the crystal quality. Figure 2(a) shows the SEM image of the surface of the 1.0-μm-thick annealed Yb:Y–Al–O film grown on c-sapphire. This film has a fine-domed surface, and there are no apparent grain boundaries at the surface. The approximate size of the domes is 100 nm in diameter. In addition, the cross-sectional SEM image of a 0.2-μm-thick annealed Yb:Y–Al–O film on c-sapphire [Fig. 2(b)] indicates that the crystal growth direction is perpendicular to the c-sapphire substrate. The Yb:Y–Al–O/c-sapphire samples thus have a zone-T structure, which is one of Thornton's structure zone models.[28] These results are consistent with both the high transparency [top inset in Fig. 1(a)] and the smooth surface of the Yb:Y–Al–O films on c-sapphire.

Thus, in the beginning of the growth of an Yb:Y–Al–O film on c-sapphire, seed crystals of Yb:YAP, Yb:YAG, and Yb:YAM are formed, and then these seed crystals grow perpendicular to the substrate at their respective intrinsic crystallization rates. As a result

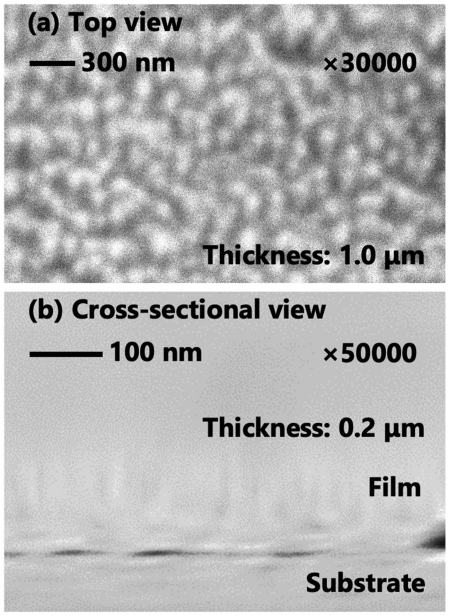

FIG. 2. SEM images of Yb:Y–Al–O films grown on c-sapphire substrates. (a) The top view of a 1.0-μm-thick annealed Yb:Y–Al–O film. (b) The cross-sectional view of 0.2-μm-thick annealed Yb:Y–Al–O film/c-sapphire.

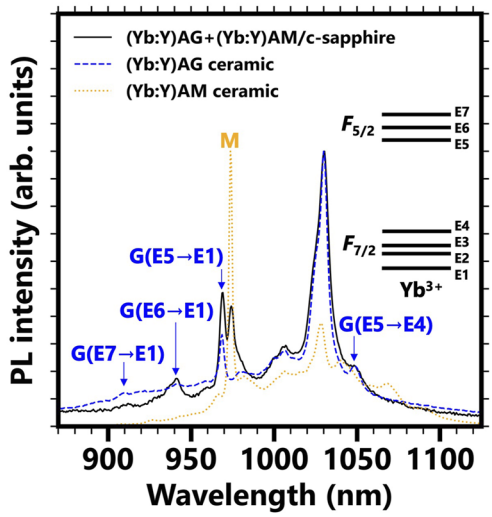

FIG. 3. PL spectra at room temperature obtained under indirect excitation of Yb^{3+} (excitation wavelength λ_{exc} = 405 nm and excitation power P_{exc} = 30.8 mW): the spectra of an annealed Yb:Y–Al–O film on c-sapphire (black solid curve), an (Yb:Y)AG ceramic (blue dashed curve), and an (Yb:Y) AM ceramic (orange dotted curve). All spectra are normalized to their respective maximum. "G" and "M" denote the PL peaks attributed to (Yb:Y) AG and (Yb:Y) AM, respectively. The diagram of seven-separated Stark levels of Yb^{3+} is shown in the inset.

of this self-organization process, the Yb:Y–Al–O/c-sapphire samples have a homogeneous columnar structure, and Yb:YAG becomes the dominant phase as the film becomes thicker because the crystallization rate during annealing of Yb:YAG is higher than the other crystallization rates under our experimental conditions. Generally, such columnar structures include mainly single crystals with high purity.[28]

D. PL spectra obtained under indirect excitation conditions

The f–f intra-orbital electric dipole transition of a single RE ion is basically prohibited, and this behavior can be mathematically described by an odd operator (the Laporte selection rule). However, an RE ion that is doped into a crystal exhibits an intrinsic PL spectrum with narrow peaks because the surrounding crystal field alters the wave function of the shielded 4f electron, and then the selection rule of the f–f intra-orbital dipole transition is slightly relaxed. Therefore, the PL due to f–f intra-orbital transitions of an RE ion reflects the intrinsic local structure of the host crystal.

Figure 3 shows the PL spectra at room temperature obtained under indirect excitation of Yb^{3+} ions, that is, PL due to the excitation of Yb^{2+} at λ_{exc} = 405 nm (excitation power P_{exc} = 30.8 mW) and a charge transfer from Yb^{2+} to Yb^{3+}.[29] The black solid curve is the PL spectrum of an annealed Yb:Y–Al–O film on c-sapphire with 1.0 μm thickness. The sputtered film does not show detectable PL signals, as well as the annealed sample. For reference, PL spectra of Yb-doped YAG (blue dashed curve) and Yb-doped YAM single-phase ceramics (orange dotted curve) are also shown. The reference samples were prepared by the solid-state reaction method from high-purity (>99.9%) raw materials of Yb_2O_3, Y_2O_3, Al_2O_3, and polyvinyl alcohol (1.5wt. %). All spectra are normalized to their respective maximum. The notation (Yb:Y) AX (X = G for garnet and M for monoclinic) is used to specify the dopant site. The PL spectrum of (Yb:Y) AM contains signals from four intrinsic RE sites with different coordination numbers and symmetries.[30]

The PL peaks of the Yb:Y–Al–O film at 913, 940, 968, and 1048 nm are attributed to the resonant transitions E7 → E1, E6 → E1, E5 → E1, and E5 → E4 of (Yb:Y) AG (Fig. 3; blue arrows), respectively. The peak at 974 nm (labeled "M") is attributed to the strong luminescence peak of Yb^{3+} ions in (Yb:Y) AM.[30] In addition, there is no signature coming from other luminescent centers, such as Yb^{3+} ions in Yb_2O_3.[31] These results are consistent with the observation of phase separation in Secs. III A–III C.

IV. RESULTS AND DISCUSSION II: Yb:YAM

In order to discuss the anti-Stokes PL properties of Yb:Y–Al–O/c-sapphire samples, we first need to clarify the unique anti-Stokes PL properties of Yb:YAM. Yb:YAM has four unique RE sites: a previous spectroscopic investigation of Yb:YAM single crystals suggested that the so-called B site in Yb:YAM [M(B)] and the C site in Yb:YAM [M(C)] are octahedrally coordinated by six oxygen ions and the so-called A site [M(A)] and D site [M(D)] are coordinated by seven oxygen ions (in polyhedral coordination with a slight derivation from inversion symmetry).[30] The energy transfer from M(D) to other sites has been observed in Yb:YAM single crystals,[30] and our previous experimental results for Yb:YAP and Yb:YAG suggest that energy transfer processes play a key role in solid-state laser cooling at high temperatures.[19,32]

To identify the relationship between the absorption and emission peaks of the Yb^{3+} ions at the four different RE-sites of YAM, we measured the PLE image of an Yb:YAM single-phase ceramic [Fig. 4(a)]. In this PLE image, the horizontal axis shows the luminescence wavelength, and the vertical axis shows the excitation wavelength λ_{exc}. The measurement was performed at 7.2 K because phonon scattering at 300 K prevents us from distinguishing the satellite peaks of the Yb^{3+} ions with different coordination numbers. The range of excitation power P_{exc} in this PLE image measurement was 2.20–2.48 mW. There are three resonant PLE signals shown in Fig. 4(a); the peaks that appear at λ_{exc} = 972.41, 973.87, and 975.43 nm are due to the Yb^{3+} ions at M(B), M(C), and M(D), respectively.[30] Corresponding to these values, there are two distinguishable anti-Stokes PL peaks near 973 and 976 nm [the spectra are shown in Fig. 9(a)], which are anti-Stokes signals of the Yb^{3+} ions at M(B) and M(C) [M(B,C)] and at M(D), respectively. The PLE signal of M(A) is not in the detectable range. However, the absorption due to M(A) may be negligible because the PL intensity is 10 times weaker than that of the other sites.

Figure 4(b) plots the PL spectra for the above-mentioned three different λ_{exc} values. We can confirm that the PL spectrum of M(B) at 7.2 K is similar to that of M(C). This similarity reflects the twin-like local structures of M(B, C). In addition, the PL spectrum of M(D) at 7.2 K shows a relatively strong PL peak at ≈1030 nm with a tail structure on the long-wavelength side. Based on the reciprocal relationship between fluorescence and absorption in the case of f–f intra-orbital transitions in trivalent RE ions, this PL peak indicates resonant absorption around 1030–1035 nm by M(D). In fact, as shown in Fig. 5, the integrated anti-Stokes PL intensity of the peak near 976 nm in the Yb:YAM single-phase ceramic at room temperature exhibits the maximum at λ_{exc} = 1031 nm. The anti-Stokes PL

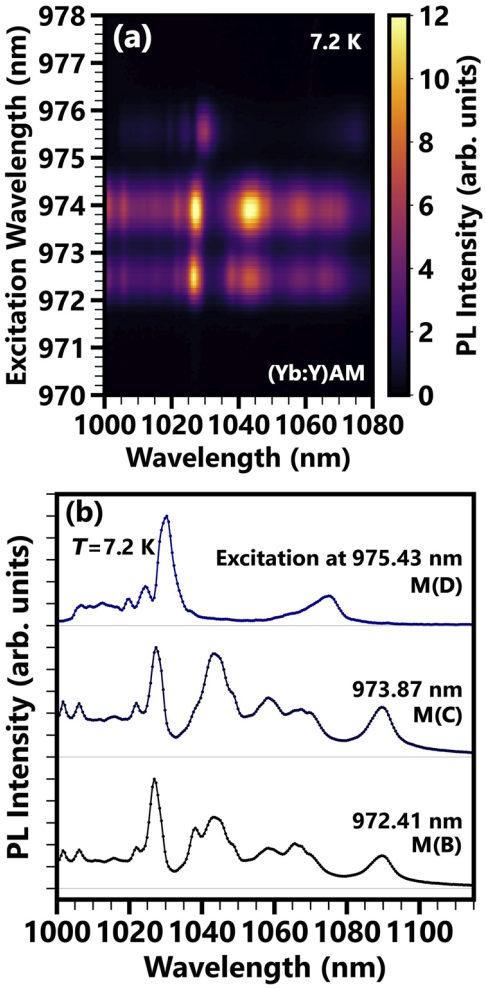

FIG. 4. (a) PLE image of an (Yb:Y) AM single-phase ceramic at 7.2 K. The selective excitation of the Yb^{3+} ions at the different sites, that is, M(B), M(C), and M(D), results in three PLE peaks due to resonant excitation. (b) The PL spectra of M(B), M(C), and M(D) obtained under resonant excitation at 972.41, 973.87, and 975.43 nm, respectively. The solid horizontal lines are baselines corresponding to zero intensity.

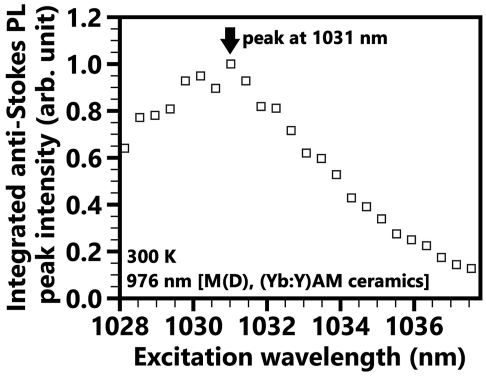

FIG. 5. Excitation wavelength dependence of the integrated anti-Stokes PL intensity of the peak near 976 nm for an (Yb:Y) AM single-phase ceramic at 300 K. The origin of the probed anti-Stokes PL peak near 976 nm is the Yb^{3+} ion at M(D).

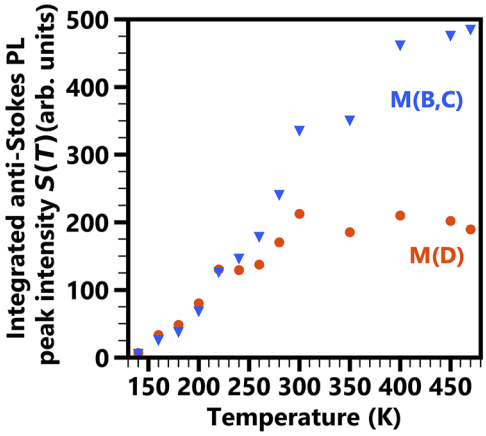

FIG. 6. Temperature dependence of integrated anti-Stokes PL peak intensities of Yb^{3+} ions at different sites for the (Yb:Y) AM single-phase ceramic (λ_{exc} = 1031 nm). The orange closed circles and blue upside-down triangles indicate the signals of Yb^{3+} ions at M(B, C) and M(D), respectively.

excitation spectrum of Yb:YAM shown in Fig. 5 was taken with an excitation power P_{exc} of 31.9–37.0 mW.

The blue upside-down triangles and the orange closed circles in Fig. 6 show the temperature dependences of the integrated anti-Stokes PL intensities of the two peaks near 973 and 976 nm, respectively. The Yb^{3+} ions in Yb:YAM were excited at λ_{exc} = 1031 nm (P_{exc} = 37.0 mW). Up to 300 K, the integrated anti-Stokes PL peak intensities increase with temperature due to the increased phonon population. However, above 300 K, the signal of M(D) tends to saturate while that of M(B, C) increases up to 470 K. These results suggest an effective energy transfer from M(D) to Yb^{3+} ions at other sites in Yb:YAM above 300 K.

V. RESULTS AND DISCUSSION III: ANTI-STOKES PL PROPERTIES AND COOLING EFFICIENCY OF Yb:Y–Al–O/c-SAPPHIRE

Figure 7 shows the anti-Stokes PL spectrum of a 1.0-μm-thick Yb:Y–Al–O film on c-sapphire at 300 K for direct excitation of Yb^{3+} at 1019 nm. The excitation power P_{exc} was 33.9 mW. We confirmed that the anti-Stokes PL intensity linearly increases with the excitation power P_{exc} and the anti-Stokes PL via the cooperative effect of the Yb-pair in the blue emission wavelength region was not observed in the thin film. The two anti-Stokes PL peaks at 968 and 974 nm involve phonon annihilation processes in Yb:YAG and Yb:YAM, respectively. The relative intensities of these peaks are different from those observed under the indirect excitation (see Stokes PL in Fig. 3). Furthermore, the ratio between the two peak intensities depends on λ_{exc}, as shown in the anti-Stokes PLE image in Fig. 8(a). Figure 8(b) shows the λ_{exc} dependence of integrated anti-Stokes PL peak intensities of different samples with a moderate excitation power range of P_{exc} = 30.3–37.2 mW. The upper panel compares the data of the Yb:Y–Al–O film on c-sapphire (open circles) with those of the Yb:YAG ceramic (blue stars) for the peak at 968 nm. The lower panel compares the data of the Yb:Y–Al–O film with those of the Yb:YAM ceramic (orange diamonds) for the peak at 974 nm. These anti-Stokes PLE spectra are normalized to their respective maximum.

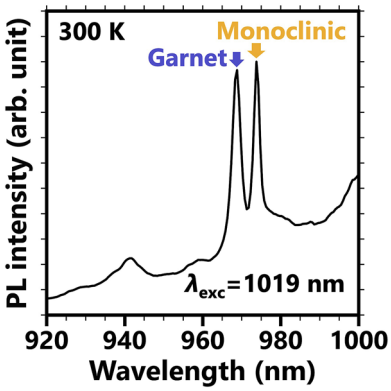

FIG. 7. Anti-Stokes PL spectrum of a 1.0-μm-thick annealed Yb:Y–Al–O film on c-sapphire at 300 K for λ_{exc} = 1019 nm. The origins of the anti-Stokes PL peaks at 968 and 974 nm are the E5 → E1 transitions in the Yb:YAG and Yb:YAM crystals in the film, respectively.

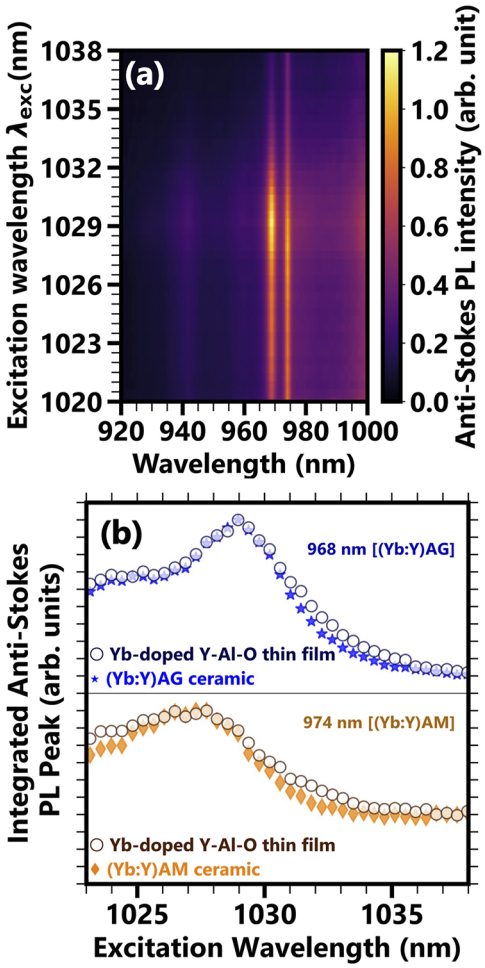

FIG. 8. (a) PLE image for the1.0-μm-thick annealed Yb:Y–Al–O film on c-sapphire at 300 K. The anti-Stokes PL peaks at 968 and 974 nm are from the (Yb:Y) AG and (Yb:Y) AM crystals in the film, respectively. (b) The excitation wavelength dependence of the integrated anti-Stokes PL intensities of the peaks at 968 and 974 nm for the Yb:Y–Al–O/c-sapphire sample (open circles), an (Yb:Y) AG ceramic (blue stars), and an (Yb:Y) AM ceramic (orange diamonds). These anti-Stokes PLE spectra are normalized to their respective maximum. The solid horizontal line is the baseline corresponding to zero intensity.

As shown in Fig. 8(b), the normalized anti-Stokes PLE intensities of 1.0-μm-thick annealed Yb:Y–Al–O/c-sapphire in the range λ_{exc} = 1030–1035 nm are higher than those of the single-phase ceramics in the same range. In general, however, the PLE spectrum arising from an f–f transition of an Yb^{3+} ion in the intrinsic crystal field is insensitive to the fabrication method. One possible reason for the broader anti-Stokes PLE spectra of Yb:Y–Al–O/c-sapphire is the energy transfer between Yb^{3+} ions in neighboring columnar crystals.

Regarding (Yb:Y) AG, there is no significant absorption beyond 1030 nm, and therefore, the Yb^{3+} ion in YAM is the candidate for the energy donor. We consider that M(D) is resonantly excited at 1030–1035 nm; then, the energy is transferred to other Yb^{3+} ions in the dodecahedron of the garnet structure and/or to M(B) and

M(C) via phonon absorption. The difference between the luminescence energies of M(D) and the other sites of the Yb^{3+} ion considered here is less than 10 meV (84.7 cm^{-1}), and thus, we consider acoustic-phonon absorption.

Figure 9(a) shows the anti-Stokes PL spectra of the Yb:YAM single-phase ceramic (orange curve) and the 1.0-μm thick annealed Yb:Y–Al–O film on c-sapphire (black curve) at 300 K for λ_{exc} = 1031 nm (P_{exc} = 37.1 mW), i.e., resonant excitation of the Yb^{3+} ions at M(D). The anti-Stokes PL spectrum of the Yb:YAM single-phase ceramic has peaks at 974 nm [corresponding to M(B, C)] and at 976 nm [corresponding to M(D)]. In contrast, Yb:Y–Al–O/c-sapphire does not show an anti-Stokes PL peak from M(D). On the other hand, in the PL spectrum at 7.5 K under indirect excitation conditions at 405 nm (P_{exc} = 40.8 mW) [Fig. 9(b)], we can clearly confirm the presence of M(D) in Yb:Y–Al–O/c-sapphire.

One possible explanation for the absence of an M(D)-related anti-Stokes PL peak in the spectrum of the Yb:Y–Al–O film in Fig. 9(a) is the fast energy transfer process from M(D) to the other Yb^{3+} ions in Yb:Y–Al–O. According to the Förster energy transfer model, the typical resonant energy transfer rate for quadrupole–quadrupole interactions between RE ions in a host

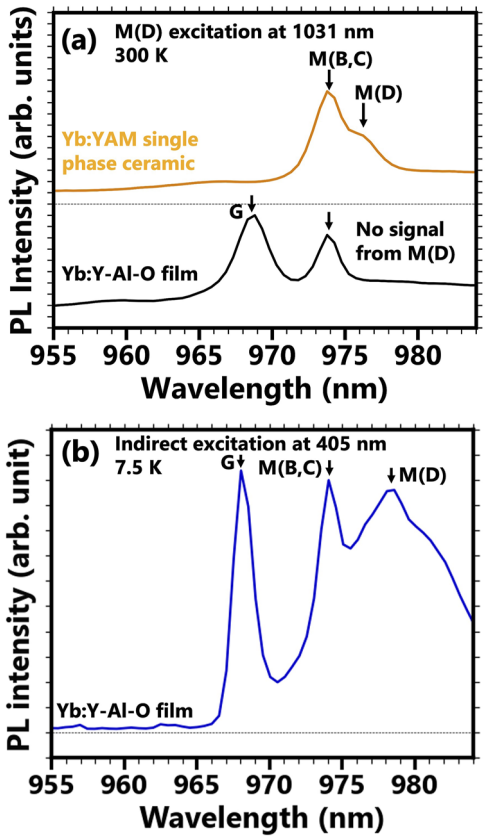

FIG. 9. (a) Anti-Stokes PL spectra of an Yb:YAM single-phase ceramic (orange curve) and a 1.0-μm thick annealed Yb:Y–Al–O film on c-sapphire (black curve) at 300 K for λ_{exc} = 1031 nm. (b) PL spectrum of same Yb:Y–Al–O film on c-sapphire at 7.5 K for λ_{exc} = 405 nm. The dotted horizontal lines are baselines corresponding to zero intensity.

crystal (~10^8 s^{-1}[33,34]) is much higher than the typical radiative relaxation rate for f–f transitions in an RE ion (~10^2 s^{-1}) and is higher than that for dipole–dipole and dipole–quadrupole interactions. Therefore, the energy of the resonantly excited M(D) can be transferred to Yb^{3+} ions in neighboring columnar crystals via acoustic-phonon absorption/creation before radiative relaxation at M(D) takes place. As a consequence of the phonon-assisted energy transfer, the anti-Stokes PLE spectra of the garnet phase [Fig. 8(b); top panel] and of M(B, C) [Fig. 8(b); bottom panel] are broader in Yb:Y–Al–O/c-sapphire. Hence, the laser cooling power can be slightly higher due to the increased acoustic-phonon absorption.

In an ideal system that has unity external quantum efficiency and less background absorption by impurities, when the mean fluorescence wavelength of PL is shorter than the excitation wavelength, laser cooling is possible, and the ideal laser cooling efficiency becomes greater than zero.[13] After subtracting the component of excitation light from the PL spectrum, the ideal laser cooling efficiency of 1.5% was obtained.[35] This positive ideal laser cooling efficiency indicates that the net cooling of this film is possible under ideal conditions.

To increase the cooling efficiency of the Yb:Y–Al–O thin film toward net cooling, improving the sample quality is one of the crucial ways. Because the Lambert law suggests that the reabsorption of fluorescence is significantly small in the 1.0-μm-thick thin film, impurities are the only main-loss source. In addition, site-selective doping of Yb^{3+} ions into the D site of Yb:YAM can enhance the cooling efficiency due to its low energy absorption at 1075 nm and considerable fast energy transfer to the cooling center. The increased absorption by Yb^{3+} results also in lower transmission loss and suppression of mean background absorption.

VI. CONCLUSION

We have discussed the anti-Stokes PL properties of Yb:Y–Al–O films grown on c-sapphire substrates. Yb:Y–Al–O films were grown by radio-frequency magnetron sputtering using a single-phase yttrium aluminum polycrystal sputtering target, and we confirmed perovskite, garnet, and monoclinic phases in the annealed films. As the mismatch between the thermal expansion coefficients of Yb:Y–Al–O and c-sapphire is small, the Yb:Y–Al–O films that were grown on c-sapphire substrates had no cracks and had better transparency than the film deposited on the fused-quartz substrate. The thin films on c-sapphire had a relatively smooth surface and consisted of densely packed sub-micron columnar crystals aligned perpendicular to the substrate. The excitation wavelength dependence of the anti-Stokes PL indicated a resonant energy transfer from Yb^{3+} ions at a specific seven-coordinated site of Yb:YAM [i.e., at M(D)] to Yb^{3+} ions in neighboring columnar crystals. We have explained that this resonant energy transfer can be faster than the radiative relaxation of the energy donor site. This energy transfer process, which is accompanied by absorption of acoustic phonons, may contribute to the enhancement of the laser cooling power.

AUTHOR DECLARATIONS

Conflict of Interest

The authors have no conflicts to disclose.

DATA AVAILABILITY

The data that support the findings of this study are available from the corresponding authors upon reasonable request.

REFERENCES

[1] R. I. Epstein, M. I. Buchwald, B. C. Edwards, T. R. Gosnell, and C. E. Mungan, Nature **377**, 500–503 (1995).
[2] B. C. Edwards, M. I. Buchwald, and R. I. Epstein, Rev. Sci. Instrum. **69**(5), 2050–2055 (1998).
[3] M. P. Hehlen, J. Meng, A. R. Albrecht, E. R. Lee, A. Gragossian, S. P. Love, C. E. Hamilton, R. I. Epstein, and M. Sheik-Bahae, Light: Sci. Appl. **7**, 15 (2018).
[4] R. Vicente, G. Nogues, J.-M. Niot, T. Wiertz, P. Contini, and A. Gardelein, Cryogenics **105**, 103000 (2020).
[5] S. R. Bowman, IEEE J. Quantum Electron. **35**(1), 115–122 (1999).
[6] M. P. Hehlen, Proc. SPIE **7228**, 72280E (2008).
[7] D. V. Seletskiy, R. Epstein, and M. Sheik-Bahae, Rep. Prog. Phys. **79**, 096401 (2016).
[8] M. Sheik-Bahae and R. I. Epstein, Phys. Rev. Lett. **92**(24), 247403 (2004).
[9] S. Zhang, M. Zhukovskyi, B. Jankó, and M. Kuno, NPG Asia Mater. **11**, 54 (2019).
[10] A. Kastler, J. Phys. Radium **11**(6), 255–265 (1950).
[11] S. Rostami, A. R. Albrecht, A. Volpi, and M. Sheik-Bahae, Photonics Res. **7**(4), 445–451 (2019).
[12] J. Fernandez, A. J. Garcia-Adeva, and R. Balda, Phys. Rev. Lett. **97**(3), 033001 (2006).
[13] R. I. Epstein, J. J. Brown, B. C. Edwards, and A. Gibbs, J. Appl. Phys. **90**(9), 4815–4819 (2001).
[14] C. B. Layne, W. H. Lowdermilk, and M. J. Weber, Phys. Rev. B **16**(1), 10–20 (1977).
[15] M. P. Hehlen, M. Sheik-Bahae, R. I. Epstein, S. D. Melgaard, and D. V. Seletskiy, J. Mater. Chem. C **1**(45), 7471–7478 (2013).
[16] S. D. Melgaard, A. R. Albrecht, M. P. Hehlen, and M. Sheik-Bahae, Sci. Rep. **6**, 20380 (2016).
[17] Z. Yang, J. Meng, A. R. Albrecht, and M. Sheik-Bahae, Opt. Express **27**(2), 1392–1400 (2019).
[18] X. Zhan, Z. Li, B. Liu, J. Wang, Y. Zhou, and Z. Hu, J. Am. Ceram. Soc. **95**(4), 1429–1434 (2012).
[19] Y. Nakayama, Y. Harada, and T. Kita, Appl. Phys. Lett. **117**(4), 041104 (2020).
[20] S. Melgaard, D. Seletskiy, V. Polyak, Y. Asmerom, and M. Sheik-Bahae, Opt. Express **22**(7), 7756–7764 (2014).
[21] G. Nemova and R. Kashyap, J. Lumin. **164**, 99–104 (2015).
[22] A. T. M. A. Rahman and P. F. Barker, Nat. Photonics **11**, 634–638 (2017).
[23] J. Knall, P.-B. Vigneron, M. Engholm, P. D. Dragic, N. Yu, J. Ballato, M. Bernier, and M. J. F. Digonnet, Opt. Lett. **45**(5), 1092–1095 (2020).
[24] W.-H. Chao, R.-J. Wu, and T.-B. Wu, J. Alloys Compd. **506**(1), 98–102 (2010).
[25] X. Xu, Z. Zhao, J. Xu, and P. Deng, Solid State Commun. **130**(8), 529–532 (2004).
[26] W. M. Yim and R. J. Paff, J. Appl. Phys. **45**(3), 1456–1457 (1974).
[27] Y. Shi, D. Ma, A. P. Song, B. Wheaton, M. Bauchy, and S. R. Elliott, J. Non-Cryst. Solids **528**, 119760 (2020).
[28] J. A. Thornton, J. Vac. Sci. Technol. **11**(4), 666–670 (1974).
[29] S. Rydberg and M. Engholm, J. Appl. Phys. **113**(22), 223510 (2013).
[30] M. Kaczkan, M. Malinowski, A. Suchocki, D. A. Pawlak, and S. Turczyński, J. Alloys Compd. **842**, 155893 (2020).
[31] V. Peters, "Growth and spectroscopy of ytterbium-doped sesquioxides," Ph.D. thesis, Universität Hamburg, 2001.
[32] Y. Nakayama, Y. Harada, and T. Kita, Opt. Express **27**(24), 34961–34973 (2019).
[33] N. Yamada, S. Shionoya, and T. Kushida, J. Phys. Soc. Jpn. **32**(6), 1577–1586 (1972).
[34] T. Kushida, J. Phys. Soc. Jpn. **34**(5), 1327–1333 (1973).
[35] Y. Nakayama, N. Nakagawa, Y. Harada, and T. Kita, J. Soc. Mater. Sci. Jpn. **69**(10), 727–732 (2020).